Angular Remanence and Anisotropy Orientation Distribution in Nickel Films on $LiNbO_3$

Scott A. Mathews, Olaf M. J. van't Erve, Mehmet A. Noyan, and Nicholas A. Charipar

Naval Research Laboratory, Materials Science and Technology Division, Washington, DC 20375 USA

Nickel thin films (100 nm) deposited on 128° *Y*-cut: $LiNbO_3$ exhibits a well-defined, uniaxial, magnetic anisotropy after annealing at 325 °C. Simulating the magnetization of these films using a temperature-dependent Stoner–Wohlfarth (SW) model indicates that the films have a very narrow angular distribution of anisotropy axis orientations. Here, we report a direct measurement of the angular distribution of anisotropy orientation by measuring the angular remanence after magnetic saturation. When magnetized to saturation in any direction away from the hard axis, these samples remain nearly uniformly magnetized, with the easy axis remnant magnetization very close to the saturation magnetization ($>0.97M_S$). When the angle (α) between the saturating field and the hard axis is $|\alpha| < 1°$, the easy axis remanence drops dramatically, indicating that the sample is no longer uniformly magnetized and has broken up into domains. When magnetized on the hard axis, the easy axis remanence approaches zero. The angular range over which the easy axis remanence drops significantly is a measure of the angular distribution of the anisotropy axes. The full-width at half-maximum (FWHM) of the easy axis remanence as a function of angle (α) is approximately 0.44° for annealed nickel thin films on 128° *Y*-cut: $LiNbO_3$. The angular remanence is modeled numerically, assuming an ensemble of SW particles with a distributed anisotropy orientation. The magnetic domain structure of the films is confirmed by magneto-optic Kerr effect imaging.

Index Terms— **Angular remanence, transverse remanence, uniaxial anisotropy.**

I. Introduction

THIN films of elemental nickel, deposited on $LiNbO_3$, and subsequently annealed at 325 °C, show a pronounced, in-plane, uniaxial anisotropy [1]. Under appropriate conditions, these films exhibit magnetic properties consistent with the Stoner–Wohlfarth (SW) model [2], including the crossing of hysteresis branches [3] and the so-called Aharoni singularity [4], [5]. When magnetized to saturation in any direction away from the hard axis, these samples remain nearly uniformly magnetized, with an easy axis magnetization greater than 97% of the saturation magnetization. In this sense, these samples act as though they are macroscopically large, single domain particles. When magnetized to saturation on the hard axis, these samples break up into domains and the easy axis remanence vanishes. Previous works have modeled the magnetic properties of these samples as an ensemble of SW particles (single domain particles) with a narrow distribution of anisotropy orientations and anisotropy magnitudes [3], [5].

Here, we report direct measurements to quantify the angular distribution of the in-plane anisotropy in these samples using the angular remanence technique [6]. Angular remanence measurements are performed in a conventional, single-axis vibrating sample magnetometer (VSM), as opposed to similar methods of measuring anisotropy distribution which rely on torque magnetometers [7], [8]. Because the angular remanence technique is insensitive to the distribution of anisotropy magnitude, this technique allows a direct estimation of the distribution of anisotropy orientation.

II. Theory and Modeling

Consider an ensemble of noninteracting, single domain particles with all easy axes lying in a plane. We assume a narrow distribution of easy axes, symmetric around the y-axis, such that the average easy axis of the ensemble is coincident with the y-axis. Assume an applied magnetic field sufficient to saturate all particles in the ensemble is applied at an angle α with respect to the x-axis, the average hard axis. A specific particle in the ensemble, with the easy axis inclined at an angle φ with respect to the y-axis, is shown in Fig. 1. We note that the elliptical shape drawn in Fig. 1 is meant to illustrate the symmetry of the anisotropy, and not necessarily the actual particle shape.

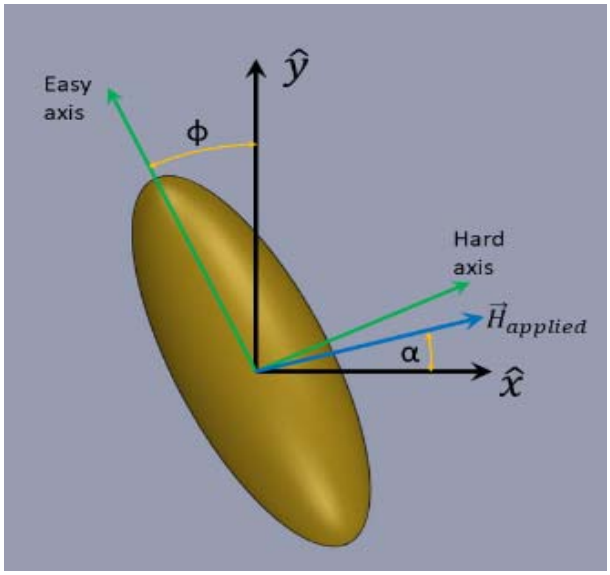

Fig. 1. Magnetic geometry for a single SW particle, oriented at an angle of φ with respect to the average easy axis. Note that the elliptical shape is a notional representation of anisotropy, and is not intended to imply shape anisotropy, exclusively.

After saturation, the magnetization will rotate to the nearest, easy axis. As a result, the reduced remanence (M_R/M_S) of the given particle along the average easy axis will be $-\cos\varphi$ if

Manuscript received September 9, 2021; accepted September 22, 2021. Date of publication September 27, 2021; date of current version November 18, 2021. Corresponding author: S. A. Mathews (e-mail: scott.mathews@nrl.navy.mil).

Color versions of one or more figures in this article are available at https://doi.org/10.1109/TMAG.2021.3115945.

Digital Object Identifier 10.1109/TMAG.2021.3115945

$\varphi > \alpha$, and cosφ if $\varphi < \alpha$. If $P(\varphi)$ is the probability of a single particle having its easy axis inclined at an angle φ with respect to the y-axis, then the easy-axis remanence of the ensemble is given by

$$m_R^{\text{ea}}(\alpha) = \int_{-\pi/2}^{\alpha} \cos\varphi P(\varphi) d\varphi - \int_{\alpha}^{\pi/2} \cos\varphi P(\varphi) d\varphi \quad (1)$$

where m_R^{ea} is a number between -1 and $+1$.

This equation can be integrated numerically, assuming an appropriate distribution function, $P(\varphi)$, and compared with the measured, easy-axis, remanence.

III. Experiment

A. Sample Preparation

Nickel films were deposited by dc magnetron sputtering on polished 128° Y-cut $LiNbO_3$ substrates. The nickel layers were between 90 and 100 nm thick, as measured by stylus profilometery. A 2 nm tantalum capping layer was deposited by dc magnetron sputtering, without breaking vacuum, in order to prevent the formation of nickel oxide on the surface. Samples were thermally annealed under vacuum ($<10^{-6}$ torr) at 325 °C for 2 h. To avoid the effects of in-plane shape anisotropy, samples were subsequently patterned into 7 mm disks using conventional photolithography and wet etch. X-ray diffraction measurements indicate that the nickel films are polycrystalline, with no strong texture or preferred orientation with respect to the substrate.

B. Angular Remanence Measurements

All angular remanence measurements were performed in a commercial, single-axis VSM. The VSM system included an automated sample rotation stage with 0.1° resolution. All VSM measurements were performed in the plane of the film, with the axis of rotation perpendicular to the plane of the film. Measurements were performed at room temperature. Because these samples have a strong uniaxial anisotropy and the measurements were made close to the hard axis, the process of centering or "saddling" the sample in the pick-up coils was crucial, as pointed out by Hanmin *et al.* [9]. Once the sample was well-saddled, a series of M–H-curves were acquired in order to determine the orientation of the average easy axis. The hard axis was determined to be 90° from the easy axis.

The easy-axis remnant magnetization was then measured as a function of angle (α). For each angle, α, from the hard axis, the field was ramped up to a value sufficient to saturate the sample (1000 Oe). The field was then ramped to zero and the sample was rotated back to the average easy axis. The remnant magnetization was measured on the average easy axis. The process was repeated for a series of α angles symmetric about the hard axis.

C. Kerr Microscope Images

Kerr microscopy images of magnetic domains were acquired using a custom-built Kerr microscope, based on a commercial, *Zeiss Axio*, polarized light microscope. Domain images were acquired in a longitudinal magneto-optic Kerr effect (MOKE) configuration, using a 40× objective. The Kerr microscope is equipped with an electromagnet capable of applying a field up to 1000 Oe, in the plane of the film. While the Kerr microscope was equipped with a sample rotation stage, the angular scale was too coarse to allow precise measurements of the sample angle. As a result, Kerr images were deliberately acquired on a region of the film that included an obvious scratch. The relative orientation of the sample was determined by measuring the angle of the scratch with image processing software (ImageJ). Background subtraction and contrast enhancement were also performed using ImageJ.

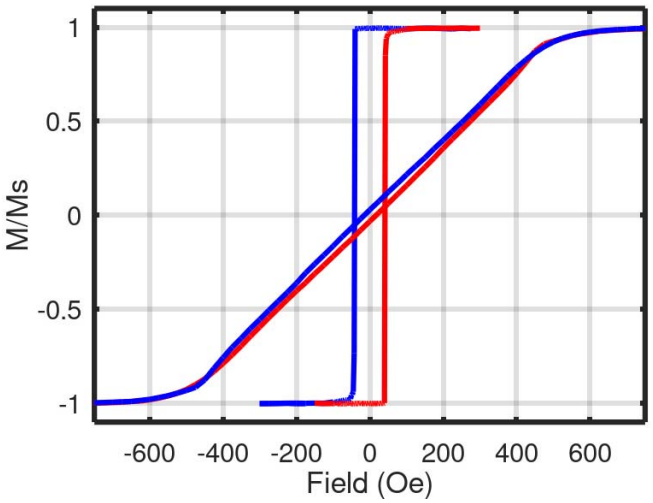

Fig. 2. M–H-loop on the hard and easy axis: reduced magnetization (M/M_S) versus applied field, with the field applied at $\alpha = 0°$ and 90°. The ascending and descending branches of the hysteresis loop are shown in red and blue, respectively.

IV. Results

Fig. 2 shows the hard and easy axis M–H-loops (acquired at $\alpha = 0°$ and 90°) of a sample after low-temperature annealing, and is representative of all the samples in this study. The ascending and descending branches of the hysteresis loops are shown in red and blue, respectively. This particular sample shows a squareness ratio (M_R/M_s) of exactly 1, as measured on the easy axis. All samples in this study show a squareness ratio greater than 0.97, when measured on the easy axis. As discussed in [1], the unannealed samples show a much smaller squareness ratio and no in-plane anisotropy. Fig. 3 shows the M–H-loop of the same sample, measured at 1° from the hard axis. As discussed in [3], all the samples in this study show a hysteresis branch crossing and are well-described by a temperature-dependent SW model.

The measured, reduced remanence is shown in Fig. 4, as a function of α, the angle of the previously applied saturating field with respect to the hard axis. While the measured data and the numeric integration of (1) yield a solution very similar to an error function, or a smoothed step function, it is more informative to plot the absolute value of the reduce remanence. These data are shown in Fig. 5, where the open squares represent measured data. The numeric solutions to (1) assuming a single, Cauchy distribution and a single normal (Gaussian) for the function $P(\alpha)$ are shown in red and blue, respectively. These two simulations represent the best fit to the data, assuming single distributions. Note that neither single distribution accurately reproduces the measured data. However, the numeric solution to (1), assuming two separate normal distributions, reproduces the measured data adequately. The solid line shown in Fig. 6 represents the numeric solution for two normal distributions, each weighted by an appropriate volume fraction. The best fit to the measured data occurs assuming standard deviations of 0.30° and 10°, with volume

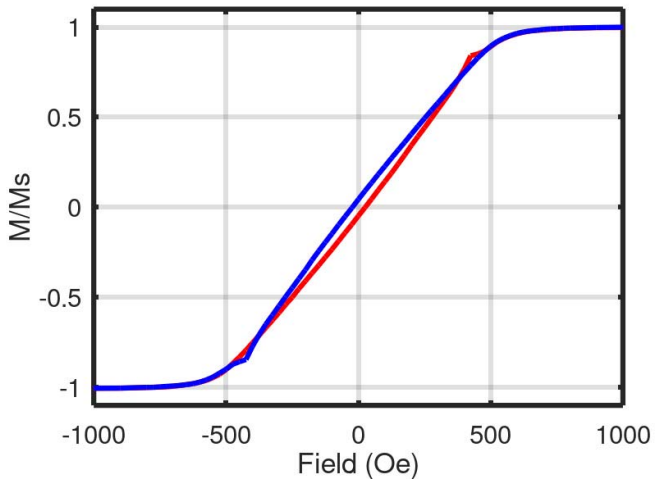

Fig. 3. M–H-loop with the field applied 1° from the average hard axis: reduced magnetization (M/M_S) versus applied field. The ascending and descending branches of the hysteresis loop are shown in red and blue, respectively. The hysteresis branch crossings are visible in both the ascending and descending branches.

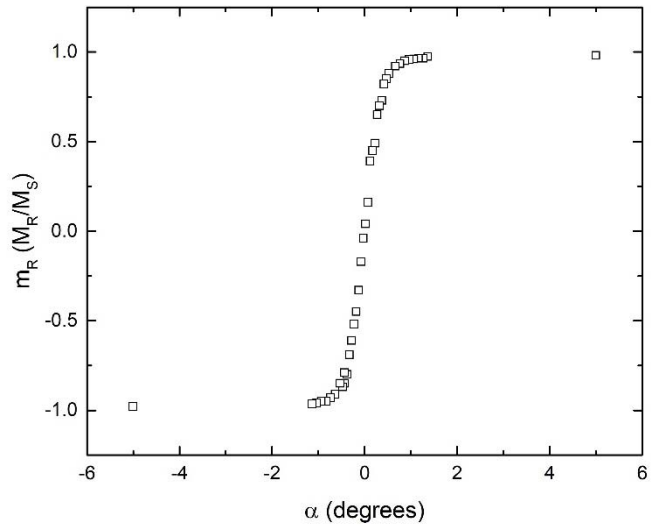

Fig. 4. Measured reduced remanence ($m_R = M_R/M_S$) on the average easy axis as a function of the angle (α) of the previously applied saturating field with respect to the average hard axis.

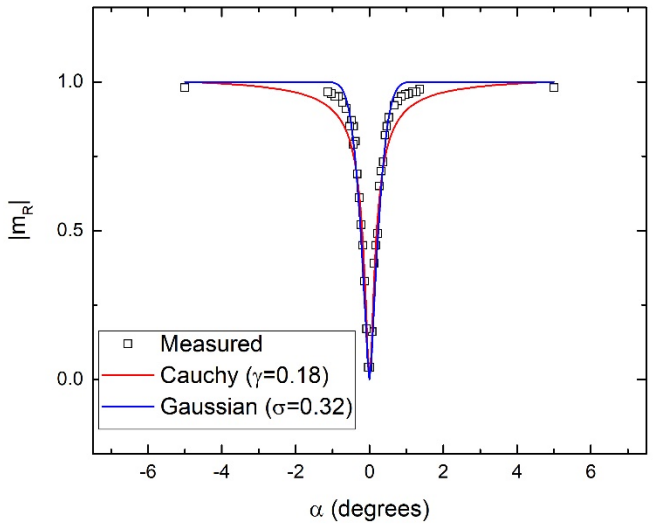

Fig. 5. Absolute value of reduced remanence ($|m_R| = |M_R/M_S|$) on the average easy axis as a function of the angle (α). Open squares represent measured data, while the red and blue lines represent the best fit of single Cauchy and Gaussian distributions, respectively.

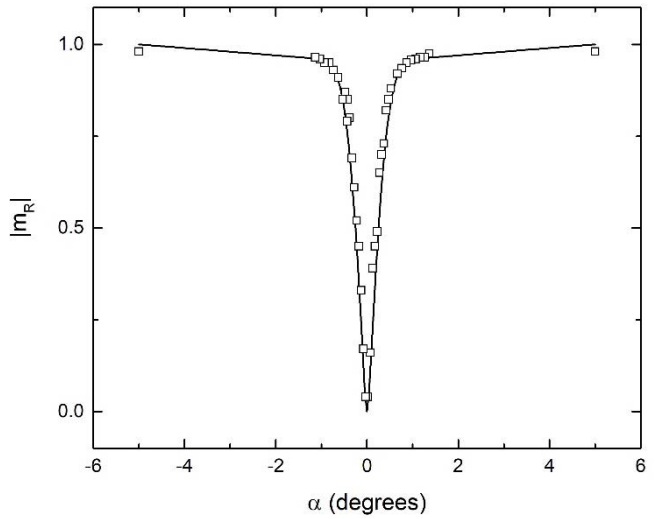

Fig. 6. Absolute value of reduced remanence ($|m_R| = |M_R/M_S|$) on the average easy axis as a function of the angle (α). Open squares represent measured data, while the solid line represents the best fit of the model, assuming a weighted average of two Gaussian distributions with standard deviations of 0.30° and 10°, and volume fractions of 0.95 and 0.05, respectively.

fractions of 0.95 and 0.05, respectively. We discuss the appropriateness of assuming two, separate, normal distributions in Section V.

Fig. 7(a)–(e) shows a series of Kerr images, acquired at zero applied field (remnant domain configuration), at various angles. The easy axis of the sample is oriented nearly vertical in these images. The saturating field, applied before the images were acquired, is nearly horizontal in these images. Fig. 7(a) shows the domain configuration at remanence after applying a saturating field approximately 1.9° from the hard axis ($\alpha = 1.9°$). Notice that no magnetic domains are visible and that the debris and imperfections appear on a light (bright) background. This is indicative of a "single domain" or uniformly magnetized remnant state. Fig. 7(b) shows the remnant domain configuration with the previously applied saturating field at 0.7° from the hard axis. A few, small, dark, elongated domains have appeared, with their long axes aligned with the easy axis of the sample. The lighter contrast represents regions where the magnetization points up, while the darker regions have magnetization pointing down. Fig. 7(c), at 0.2° from the hard axis, shows an increase in the number and areal density of the darker domains. Fig. 7(d) shows the remnant domain configuration with the saturating field essentially coincident with the hard axis. Fig. 7(e) shows the remnant domain beyond the hard axis ($\alpha = -0.4°$). In this image, the majority of the regions appear dark (magnetization pointing down).

In all the images, the stripe domains tend to be oriented vertically, along the easy axis, with significant "magnetization ripple" [10]. In addition, we note that the initial width of the domains in these images is on the order of 1–3 μm, considerably larger than the domain widths reported in the literature for nickel films of similar thicknesses [11], [12]. These images provide further confirmation that the samples remain uniformly magnetized at remanence, in a "single-domain"

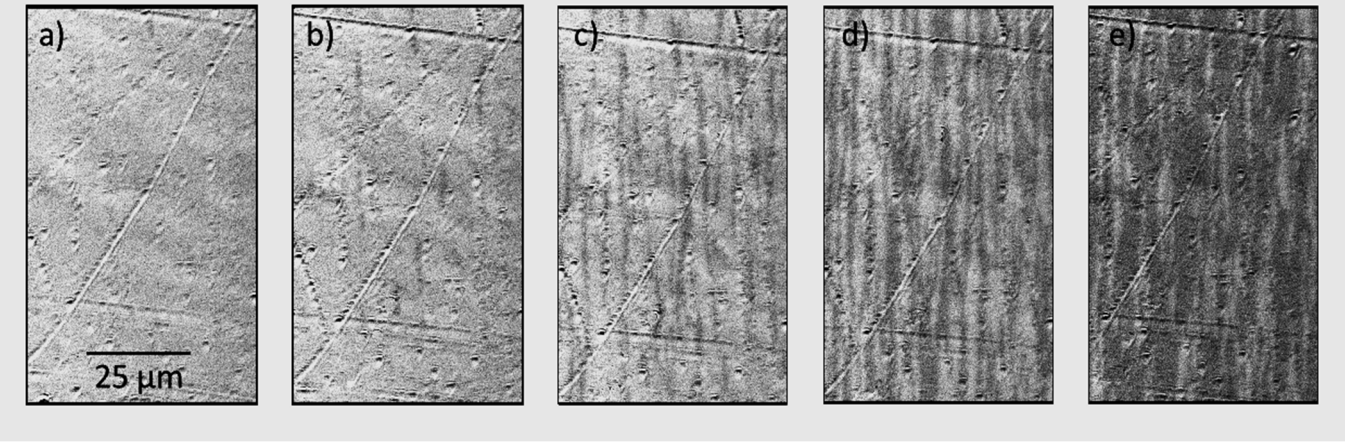

Fig. 7. (a)–(e) MOKE images of the remnant domain structure after saturating with an applied field at (a) $\alpha = 1.9°$, (b) $\alpha = 0.7°$, (c) $\alpha = 0.2°$, (d) $\alpha = 0.0°$, and (e) $\alpha = -0.4°$, as measured from the average hard axis. The easy and hard axes are approximately vertical and horizontal, respectively. Note that the domains show a stripe-like morphology, oriented along the easy axis, with "magnetization ripple."

state, when previously saturated in any direction other than the average hard axis, and that the samples break up into stripe-like domains when saturated on the average hard axis.

V. Discussion

As discussed in [1], the magnetic anisotropy in the nickel film results from a uniaxial strain created during annealing. The thermal coefficient of expansion (TCE) of the 128° Y-cut plane of $LiNbO_3$ is anisotropic, with a uniaxial symmetry. In one direction, the TCE of the film is well matched to the substrate, while in the perpendicular direction, there is a significant mismatch. Presumably, annealing the film at 325 °C for 2 h reduces internal stresses, such that the film is nearly stress free. Upon cooling to room temperature, a uniaxial strain is produced due to the mismatched TCE. The uniaxial strain leads to a uniaxial magnetic anisotropy due to magnetostriction in the nickel. Because the substrate is a single crystal, the orientation of the strain is extremely well-defined, leading to a very well-defined magnetic anisotropy.

Given that the nickel film is patterned into a disk, it is reasonable to assume that the nickel at the edges of the disk is subject to a different, nonuniform strain, as compared with the nickel in the center of the disk. Therefore, we expect a small volume fraction of the nickel, subject to a nonuniform strain, to show a wider distribution of anisotropy orientations. This accounts for the fact that the data are best fit by two distributions, one narrow and one wider, with the narrow distribution accounting for the majority of the volume of the film.

VI. Conclusion

Nickel films annealed on 128° Y-cut $LiNbO_3$ show a well-defined magnetic anisotropy. We have directly measured the distribution of the orientation of the anisotropy using the angular remanence technique. This technique probes the orientation distribution of the anisotropy and is not sensitive to the magnitude distribution. These measurements indicate that the majority of the film (95%) can be well-described by a normal distribution with a standard deviation of 0.3°, while the remainder of the volume (5%) has a standard deviation of 10°. These results demonstrate that the anisotropy orientation is extremely well-defined in these samples. MOKE images confirm that the samples remain in a "single-domain" state at remanence when magnetized away from the hard axis, and only break up into domains when the magnetizing field is less than 1° from the hard axis.

Acknowledgment

This work was supported by the Office of Naval Research through the Naval Research Laboratory 6.1 Base Program.

The authors would like to thank Dr. Allison Flatau and Dr. Jungjin Park, of the University of Maryland, for the use of their Kerr microscope.

References

[1] S. A. Mathews *et al.*, "Thermally induced magnetic anisotropy in nickel films on surface acoustic wave devices," *IEEE Trans. Magn.*, vol. 55, no. 2, pp. 1–4, Feb. 2018.

[2] E. Stoner and E. Wohlfarth, "A mechanism of magnetic hysteresis in heterogeneous alloys," *Trans. Roy. Soc. London*, vol. A240, pp. 599–644, May 1948.

[3] S. A. Mathews, A. C. Ehrlich, and N. A. Charipar, "Hysteresis branch crossing and the Stoner–Wohlfarth model," *Sci. Rep.*, vol. 10, no. 1, pp. 1–17, Sep. 2020.

[4] A. Aharoni, E. Frei, S. Shtrikman, and D. Treves, "The reversible susceptibility tensor of the Stoner–Wohlfarth model," *Bull. Res. Couns. Isr.*, vol. 6A, pp. 215–238, Apr. 1957.

[5] S. A. Mathews, C. Musi, and N. Charipar, "Transverse susceptibility of nickel thin films with uniaxial anisotropy," *Sci. Rep.*, vol. 11, no. 1, pp. 1–6, Feb. 2021.

[6] H. J. Richter and H. Hibst, "Magnetic characterization of ME tapes: The angular remanence curve," *J. Magn. Magn. Mater.*, vol. 95, no. 1, pp. 118–122, Apr. 1991.

[7] P. J. Flanders and S. Shtrikman, "Experimental determination of the anisotropy distribution in ferromagnetic powders," *J. Appl. Phys.*, vol. 33, no. 1, pp. 216–319, 1962.

[8] C. Papusoi, A. Stancu, and C. Papusoi, "Magnetic method for anisotropy axis distribution analysis," in *Magnetic Storae Systems Beyond* (NATO Science), vol. 41. Dordrecht, The Netherlands: Springer, 2001, doi: 10.1007/978-94-010-0624-8_16.

[9] J. Hanmin, S. Dongsheng, G. Cunxu, and H. Kim, "Inverted hysteresis loops: Experimental artifacts arising from inappropriate or asymmetric sample positioning and the misinterpretation of experimental data," *J. Magn. Magn. Mater.*, vol. 308, no. 1, pp. 56–60, Jan. 2007.

[10] D. B. Cullity and C. D. Graham, *Introduction to Magnetic Materials*. 2nd ed. Hoboken, NJ, USA: Wiley, 2009, pp. 407–408.

[11] P. D. Sparks *et al.*, "Stripe domains and magnetoresistance in thermally deposited nickel films," *J. Magn. Magnetic Mater.*, vol. 272, pp. E1339–E1340, May 2004.

[12] C. T. Hsieh, J. Q. Liu, and J. T. Lue, "Magnetic force microscopy studies of domain walls in nickel and cobalt films," *Appl. Surf. Sci.*, vol. 252, no. 5, pp. 1899–1909, Dec. 2005.